Ultrafast polarization switching via laser-activated ionic migration in ferroelectric $CuInP_2S_6$

Jin Zhang,[1,*] Kun Yang,[1] Jianxin Yu,[1] Honghao Wan,[2] Jia Zhang,[3,†] Huixia Fu,[2,‡] Zijing Ding,[4,§] Xinghua Shi,[1] and Sheng Meng[5,6]

[1]*Laboratory of Theoretical and Computational Nanoscience, National Center for Nanoscience and Technology, Chinese Academy of Sciences, Beijing 100190, People's Republic of China*

[2]*Center of Quantum Materials and Devices & Chongqing Key Laboratory for Strongly Coupled Physics, Chongqing University, Chongqing 401331, People's Republic of China*

[3]*Max Born Institut für Nichtlineare Optik und Kurzzeitspektroskopie, Berlin 12489, Germany*

[4]*Beijing Computational Science Research Center, Beijing 100193, People's Republic of China*

[5]*Beijing National Laboratory for Condensed Matter Physics, and Institute of Physics, Chinese Academy of Sciences, Beijing 100190, People's Republic of China*

[6]*Songshan Lake Materials Laboratory, Dongguan, Guangdong 523808, People's Republic of China*

(Received 26 November 2024; revised 11 February 2025; accepted 10 March 2025; published 20 March 2025)

As a layered ferroelectric material, $CuInP_2S_6$ has garnered significant attention for its robust ferroelectric state and potential applications in memory devices. In this work, we demonstrate that with short laser pulses ultrafast reversible polarization switching within hundreds of femtoseconds can be achieved in ferroelectric $CuInP_2S_6$. Specifically, photoexcitation triggers collective ionic migration and ferroelectricity reversal in $CuInP_2S_6$, revealing a different pathway to access different ferroelectric phases through optical excitation. Our findings indicate that laser pulses substantially alter the transition barriers, promoting ionic transport facilitated by the photodoping effect. This laser-induced ionic migration proves critical for enabling polarization transitions, offering a pathway to explore and control exotic quantum phases. These insights open exciting possibilities for manipulating ferroelectric states and electronic properties on an ultrafast timescale.

DOI: 10.1103/PhysRevB.111.104111

I. INTRODUCTION

Ferroelectric materials hold great potential as dielectrics in information storage and functional device applications [1–5]. These materials possess spontaneous electric polarizations below critical temperatures, which can be switched by electric fields. Layered ferroelectric materials facilitate the fabrication of ultrathin ferroic structures through exfoliation without dangling bonds. Additionally, they offer clean interfaces with other two-dimensional (2D) materials that can be modulated with external electric fields, promising for innovative electronic devices including tunnel junctions and ferroelectric field-effect transistors [6–11].

Recently, the study of ferroelectricity in 2D materials has opened up the possibilities for large-scale nanoelectronic applications [12–16]. The family of van der Waals layered ferroelectric materials, including $CuInP_2S_6$ (CIPS) and In_2Se_3, is advantageous for controlling dielectrics for nonvolatile memory, ferroelectric field-effect transistors and advanced sensors [8,17–26]. In particular, CIPS is a representative 2D ferroelectric material wherein the Cu and In atoms displace in opposite directions within each layer [8–13]. It has long been recognized for its significant ionic conductivity at elevated temperatures, primarily ascribed to ionic hopping facilitated by the coupling between ionic vibrations and lattice deformation. In addition, Sokrates and coauthors revealed that CIPS hosts a quadruple-well potential with two distinct polar phases, attributing to the out-of-plane migration of Cu ions [12]. CIPS serves as a bridge between ferroelectrics characterized by distinct polarization states and ionic conductors, which exhibit multiple potential minima for ionic displacements separated by relatively shallow energy barriers. However, the relationship between ionic migration and carrier dynamics remains largely unexplored. The present work endeavors to bridge the gap by presenting a comprehensive investigation into the unique characteristics of CIPS, shedding light on the photoexcited lattice and carrier dynamics in ferroelectric materials.

In this paper, we investigate photoexcited ultrafast polarization switching driven by ionic migration in the prototypical van der Waals ferroelectric CIPS, utilizing real-time time-dependent density functional theory (TDDFT) simulations (see more details in the Supplemental Material [27]). These calculations allow us to unravel photoinduced structural changes at the atomic scale and femtosecond timescale. Optical excitation significantly modulates the ionic transition barriers in CIPS, triggering collective ionic dynamics. Furthermore, we identify intrinsic processes of polarization transitions, unveiling that various polarization states can be achieved through laser photoexcitation. This study not only

*Contact author: jinzhang@nanoctr.cn
†Contact author: jia.zhang@mbi-berlin.de
‡Contact author: hxfu@cqu.edu.cn
§Contact author: zding@csrc.ac.cn

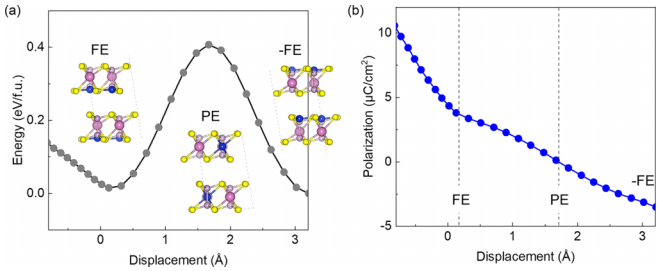

FIG. 1. Energy profile and total polarizations of CIPS at the ground state. (a) Total energies with different ionic positions. Insets show the atomic structures of CIPS with the ferroelectric state (FE) and paraelectric state (PE). The state with inversed polarization is labeled "-FE" in panel (a). The energy of the FE state is set to zero. (b) Polarizations with various Cu sites. The displacements of ferroelectric and paraelectric states are denoted by dashed lines. The energy barrier is abstained with the nudged elastic band optimization by linear interpolating along the transition path. The blue, red, purple, and yellow spheres denote Cu, In, P, and S atoms, respectively.

provides profound insight into the ultrafast phase transitions in layered ferroelectric materials but also establishes a different framework for understanding photoinduced phenomena in a wide range of quantum materials.

II. RESULTS AND DISCUSSION

Below the Curie temperature, the bulk CIPS displays a monoclinic structure with four formula units per unit cell, behaving as an insulator. The inherent relationship between ferroelectricity and substantial ionic conductivity is intuitive, as long-range ion migration tends to disrupt dipole ordering. Further analysis indicates that applying hydrostatic pressure suppresses crystal distortion and forces Cu ions into interlayer sites, thereby increasing spontaneous polarization [12]. At higher temperatures (>42 °C), Cu ions become mobile and possibly occupy both intra- and interlayer lattice positions, which leads to a disordered state with no net polarization [10,13]. Previous studies have experimentally obtained the polarization of ferroelectric CIPS to be approximately 4 $\mu C/cm^2$ [22–24]. In contrast, when Cu ions in adjacent layers move in opposite directions, the interlayer stacking results in zero macroscopic polarization, corresponding to the antiferroelectric phase [13]. Despite its moderate polarization, CIPS has recently been found to exhibit negative longitudinal piezoelectric coefficients [15].

To estimate the thermal stability, we performed *ab initio* calculations on the total energies as a function of ionic displacements in CIPS, defined by the perpendicular distance between Cu ions and the adjacent sulfur layer at the bottom. As shown in Fig. 1(a), the ferroelectric state exhibits an energy minimum at a displacement of 0.15 Å, confirming the ground-state configuration. When the displacement increases to 1.67 Å, the Cu ions move to the layer center, resulting in a state with no macroscopic polarization (i.e., the paraelectric state). The energy barrier for this phase transition was determined using nudged elastic band optimization, where intermediate structures were linearly interpolated to locate the saddle point along the transition path. We apply linear interpolation and extrapolation to obtain the transition path and atomic structures. The two energy minima (+FE and −FE states) serve as the reference points, with intermediate geometries linearly interpolated along the path and extrapolated beyond the FE state, as shown in Fig. 1(a). The barrier for the transition from the ferroelectric to the paraelectric state is 0.41 eV. For the configurations with negative displacements, Cu ions migrate into the interlayer positions or van der Waals gap, with a moderate transition barrier.

In our calculations, the ferroelectric CIPS phase exhibits a macroscopic polarization of 3.74 $\mu C/cm^2$, while the paraelectric state shows no net polarization, consistent with previous experimental and theoretical studies [22–24]. In experiments, CIPS has been found to exhibit a quadruple-well potential with two distinct polar phases (one with high polarization and the other with low polarization) [12]. The high-polarization state is characterized by an amplitude of 11.26 $\mu C/cm^2$, wherein Cu ions are displaced into the van der Waals gap. In our calculations, the polarization increases significantly when Cu ions move into the van der Waals gap, featuring a state with large polarization (10.6 $\mu C/cm^2$) for the displacement of 0.81 Å, although there is a difference in the lattice constants between our calculations and the experimental measurements. These findings reveal that polarizations are highly sensitive to ionic displacement. As exhibited in Fig. 1(b), the net polarization depends directly on the ionic displacements in ferroelectric CIPS. This analysis establishes a clear relationship between the ionic displacement and macroscopic polarization.

We note that the observed energy maximum at the PE state is not coincidental but rather a consequence of the structural symmetry along the perpendicular direction. In the FE phase, Cu ions exhibit off-center displacements, preferentially localized on the same side within each layer at the ground state. The energy maximum corresponds to the configuration in which all Cu ions are symmetrically positioned at the center of each layer, thereby resulting in zero net polarization.

Next, we conducted molecular dynamics (MD) simulations to examine the thermal effects and lattice propagation of CIPS under varying initial ionic temperatures. As demonstrated in Fig. S1 of the Supplemental Material [27], the ionic displacement amplitude increases with rising temperatures. Snapshots of the final structures after 5 ps at different temperatures are also provided. At 300 K, the displacement amplitude of Cu ions grows to 1 Å. The Cu ions become delocalized into the interlayer space with an average displacement of 0.7 Å, indicating enhanced ionic delocalization without polarization switching even at elevated temperatures. This phenomenon is attributed to the out-of-plane phonon modes of the Cu ions with the phonon frequency at around 66 cm^{-1}.

External electric fields are a conventional method for achieving polarization switching, but they face significant limitations, including the need for circuitry access and slow times on the nanosecond scale. Motivated by the above findings, we performed real-time TDDFT simulations to investigate laser-induced phase transitions in ferroelectric CIPS, capturing the intricate quantum behavior of the lattice and the evolution of excited states. As shown in Fig. 2, the photoinduced structural changes are presented under different laser photon energies. To track laser-induced dynamics in bulk CIPS, a

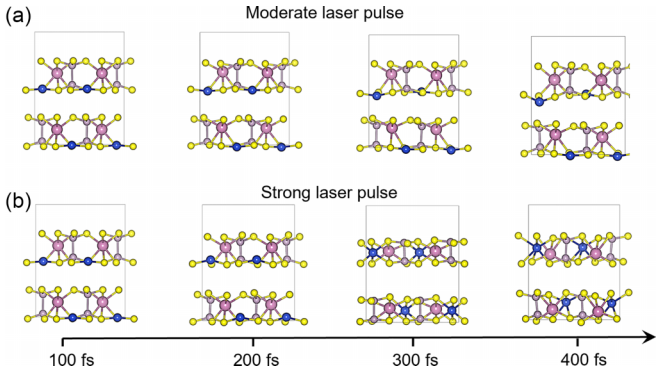

FIG. 2. Time evolution of atomic structures of bulk CIPS under photoexcitation. (a) Snapshots for time-dependent atomic structures after photoexcitation at 0, 200, 400, and 600 fs for the photon energy of 3 eV with the laser intensity $E_0 = 0.5\,\mathrm{V/Å}$, respectively. (b) The same quantity as (a) with the laser intensity $E_0 = 0.75\,\mathrm{V/Å}$.

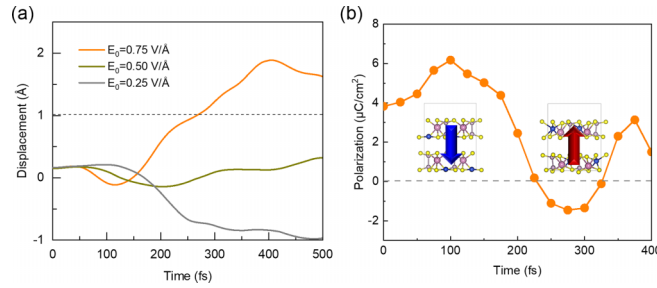

FIG. 3. Time evolution of atomic structure and polarization in CIPS under photoexcitation. (a) Perpendicular displacements of Cu ions for the intensities ranging $0.25 - 0.75\,\mathrm{V/Å}$. The applied photon energy is 3 eV. (b) Total polarizations during the evolution. The insets show the schematic phases and corresponding directions of total polarization. The dashed line denotes the states with no polarization with Cu ions in the middle of the intralayer spaces.

Gaussian-envelope function is used to describe the applied laser pulses,

$$E(t) = E_0 \cos(\omega t) \exp\left[-\frac{(t-t_0)^2}{2\sigma^2}\right], \tag{1}$$

where E_0, ω, t_0, and σ are the maximum strength, the photon energy, the peak time of the electric field, and the width of the Gaussian pulse, respectively. The band gap of CIPS is 1.45 eV on the level of the PBE functional, as illustrated in Fig. S2. Laser pulses are employed with various photon energies to excite the system and the electronic and structural evolutions are monitored after photoexcitation. Upon laser irradiation, the electronic subsystem is directly excited, initiating selective excitations of various phonon modes through electron-phonon coupling.

We further investigate ultrafast photoinduced dynamics in CIPS under various laser frequencies and intensities. At a laser field strength $E_0 = 0.25\,\mathrm{V/Å}$, a structural modulation is observed in ionic displacement with an amplitude of 1.0 Å after 500 fs for the photon energy of 3 eV. This displacement fluctuates around the value, but no polarization switching from ionic migration is detected. In contrast, at the moderate intensity $E_0 = 0.50\,\mathrm{V/Å}$, Cu ions at the bottom layer become significantly more mobile [Fig. 2(a)]. After 400 fs, it is found that a subset of ions begins to migrate toward the interlayer space while the other Cu ions localize within the bottom sites with no obvious displacement.

In contrast, the ionic distribution undergoes complete reconfiguration due to photoexcitation for the strong laser field strength $E_0 = 0.75\,\mathrm{V/Å}$ [Fig. 2(b)]. All Cu ions migrate to the center of the intralayer space at $t = 300$ fs and the ions are localized near the top layer by 400 fs, indicating that the polarization is fully switched by photoexcitation. Our calculations show that the polarization of CIPS is highly sensitive to ionic displacements. Additionally, another significant factor affecting the total polarization is laser-induced lattice deformation, which temporarily alters the interlayer distance and local potential landscape. We observe lattice deformation, evidenced by a 28% reduction in layer height along the perpendicular direction at 300 fs, followed by a quick recovery. This interplay between ionic displacements and structural deformations provides a comprehensive picture of polarization dynamics in CIPS. The Cu ions migrate into the interlayer spaces because there are two distinct polar phases while the ions move toward the intralayer assisted by the lower energy barrier for strong laser intensities [12]. This finding sharply contrasts with the traditional understanding of polarization reversal, where changes in polarization induced by an electric field are predominantly attributed to ionic displacements.

The time evolution of structures and polarizations under photoexcitation are shown in Fig. 3(a). Specifically, the ionic displacement increases for the photon energy of 3 eV with the laser intensity $E_0 = 0.75\,\mathrm{V/Å}$, surpassing the ground-state configuration with all Cu ions localized at the bottom layer. The results unveil that the ferroelectric state is destroyed in an ultrafast timescale of 250 fs. The laser-induced dynamics in bulk CIPS differ significantly from the thermally induced process. The ionic displacement is accompanied by a larger polarization, leading to the formation of a photoinduced ferroelectric state with Cu ions occupying the interlayer positions. The displacement reaches a peak of 0.32 Å at 450 fs, signaling the emergence of a different structural order. Notably, the oscillation is assigned to the phonon mode at the frequency of $66\,\mathrm{cm^{-1}}$, corresponding to the out-of-plane mode of Cu ions. The results signify that lattice vibrations play a crucial role in ferroelectric polarization switching.

Figure 3(b) illustrates the dependence of total polarization on the laser-induced ionic displacement of Cu ions in CIPS. Our simulation exhibits the polarization increased to $6.5\,\mu\mathrm{C/cm^2}$, which is accompanied by the Cu ions moving into the van der Waals gap for the first 100 fs after photoexcitation. Furthermore, the Cu ions transport along the opposite direction into the intralayer space and the detailed analysis shows that the total polarization decreases from 3.5 to $0\,\mu\mathrm{C/cm^2}$ within 400 fs and reaches an opposite polarization of $2\,\mu\mathrm{C/cm^2}$ at approximately 300 fs. Our findings demonstrate that laser pulses can significantly modulate ionic migration upon photoexcitation. The total polarization is fully switched within 400 fs, coinciding with the significant displacement of Cu ions.

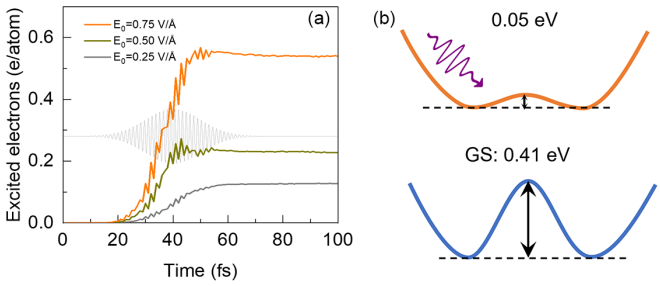

FIG. 4. Photoexcited carrier dynamics and ionic transition barriers in CIPS. (a) The number of excited electrons upon photoexcitation from the valence to conduction bands under the laser pulses. The inset shows the shape of the applied electric field along the out-of-plane direction. The photon energy is 3 eV with the polarization along the perpendicular axis, and the shape of the applied laser pulse is shown in light grey. (b) Schematic profiles of the energy barriers at the ground state (GS) and photoexcited state, respectively. Photoexcitation can effectively lower the barrier of intralayer ionic transport.

Photoexcited carriers are generated by exciting electron-hole pairs under illumination. The concentration of photoinduced carriers can effectively modulate the ionic transition barriers. To understand the modulation of ionic transition barriers, the photodoping effect is systematically examined in CIPS, specifically the time evolution of excited carrier populations. Figure 4(a) shows the number of electrons excited from the valence to the conduction bands during laser excitation. The dependence of the number of excited electrons on the laser strength is calculated by projecting the time-evolved wave functions on the basis of the ground-state wave functions. Although ground-state wave functions depend on the time-propagated atomic coordinates, the self-consistent calculations are performed using the fixed atomic structures in the ground state as the configuration experiences negligible change in the early stage within several tens of femtoseconds. For the photon energy of 3 eV, we observe a doping carrier density of 0.13 e/atom with the intensity $E_0 = 0.25\,\mathrm{V/Å}$. By contrast, the total density of excited carriers increases to $0.23\,e$/atom for $0.50\,\mathrm{V/Å}$. Additionally, the excited carrier density rises to $0.54\,e$/atom for $0.75\,\mathrm{V/Å}$. Our findings manifest that optical excitation contributes to an enhancement in charge density near the Cu ions and a noticeable depletion around the sulfur atoms. Therefore, the density of excited electrons increases with the strength of the laser field and stabilizes as the laser field diminishes.

To validate these findings, laser pulses with various photon energies are further compared (Fig. S3 [27]). Clearly, the laser pulse with a large energy of 7 eV introduces ferroelectric reversal in CIPS at the relatively small intensity of $0.25\,\mathrm{V/Å}$. The displacement decreases for the high photon energy, surpassing the ground-state configuration, reflecting that the ferroelectric state is destroyed in an ultrafast timescale of 400 fs. By contrast, the laser-induced dynamics in bulk CIPS differ markedly for the photon energy of 5 eV. The Cu ions experience small fluctuations with the laser intensity $E_0 = 0.25\,\mathrm{V/Å}$, along the perpendicular direction due to the inherent lattice rigidity. The laser-induced displacement results in increased polarization and the formation of a photoinduced ferroelectric state, with Cu ions occupying interlayer positions. The results suggest that lattice vibrations play a crucial part in the polarization change in ferroelectric CIPS.

We also illustrate the corresponding lattice temperatures after photoexcitation for the large photon energy to understand the laser-induced changes, as shown in Fig. S4. The effective temperature increases obviously due to the energy transfer from the Kohn-Sham electronic orbitals to the kinetic and static potential energy of the lattice subsystem. The concurrent ionic temperature shows that ultrafast polarization switching is not solely introduced by the lattice temperature. During this process, the lattice temperature spikes to above 500 K and then oscillates around this value. This suggests that the ionic diffusion could lead to the ferroelectric state transition when the lattice temperature surpasses its equilibrium thermal transition point. Our TDDFT-MD simulations naturally account for the damping of high-energy quasiparticles. These quasiparticles dissipate the energy to electrons at lower energy levels and the ionic subsystem. Therefore, excited electrons rapidly thermalize through electron scattering, forming a hot electron gas with an electronic temperature of several thousand K, significantly higher than that of the lattice subsystem.

It is important to note that the lattice temperature in a laser-induced nonequilibrium system differs from the equilibrium ionic temperature. The temperature comes from the kinetic energy of all ions defined as $\tilde{T} = M v_{\mathrm{ions}}^2/3k_{\mathrm{B}}$, where v_{ions} is the ion velocity, M is the atomic mass, and k_{B} is the Boltzmann constant. The large oscillation in $\tilde{T}$ is interpreted as the kinetic energy and ionic potential energy exchange coherently. Due to the small unit cell in our simulations, the temperature lacks sufficient statistical sampling. Thus, the ionic temperature cannot be directly compared with the experimental temperature for the phase transition. It is important to note that our TDDFT-MD simulations naturally account for the damping of high-energy excitations, where energies are dissipated to lower-energy carriers and the lattice subsystem (Fig. S5). However, it is essential to recognize that full equilibrium between electrons and ions is not achievable due to the limitations of the current TDDFT-MD approach [28–30].

The structural and electronic dynamics obtained from first-principles calculations provide insight into the photoinduced behavior following optical excitations in CIPS on femtosecond timescales. Furthermore, we demonstrate that the excited carriers significantly modify the ionic transition barriers, as illustrated in Fig. 4(b). The energy barriers under optical illumination are obtained using constrained density functional theory with fixed occupations. In this approach, we impose constraints on the occupation of specific electronic states by fixing the number of electrons in certain orbitals during DFT calculations (see the Supplemental Material for details [27]).

The energy barrier for Cu ion diffusion between the top and bottom sulfur layers decreases to 0.05 eV for a photodoping level of $0.3\,e$/atom, one order of magnitude smaller than the value at the ground state (0.41 eV). This unveils that the application of intense lasers and ultrafast electron-electron scattering alters the potential energy surface, potentially driving cooperative atomic motions toward a different photoinduced ferroelectric state. The excited carriers

play a pivotal role in the ferroelectric switching. Therefore, the phase dynamics can be postulated to result from both the modification of the ionic transition barrier in CIPS and the laser-induced rise in the effective temperature.

Our calculations provide direct insight into the structural and electronic dynamics following optical excitation in CIPS at femtosecond scales. Under laser illumination, strong photoexcitation generates a high density of electron-hole pairs. The excited carriers thermalize among themselves, forming a hot electron gas with a temperature higher than that of the lattice subsystem. The lattice is subsequently heated by the hot electrons via effective electron-phonon interactions. The switching of the ferroelectric state occurs when the lattice temperature exceeds its equilibrium thermal transition temperature. Additionally, the polarization reversal is enhanced by modifications of the ionic transition barriers in CIPS, leading to cooperative atomic motions that drive the ferroelectric reversal. Photoexcited carriers induce coherent ionic motions and lattice oscillations, distinct from thermally excited dynamics, and originate from energy transfer between the electronic and lattice subsystems. From a broader perspective, our results highlight the critical role of ionic migration in ferroelectric switching, suggesting that photodoping may also significantly influence ionic migration and polarization switching in van der Waals ferroelectric materials.

III. CONCLUSION

In summary, our TDDFT-MD simulations demonstrate the nature of laser-induced polarization changes and switching through ionic migration in ferroelectric CIPS, uncovering interesting collective dynamics driven by the photodoping effect, distinctly different from thermally induced polarization reversal. Our results prove that photodoping modulates the ionic transition barriers, facilitating the ultrafast reversal of the ferroelectric state in the bulk CIPS. This work offers insight into the photoinduced ferroelectric-paraelectric switching in van der Waals ferroelectric materials and suggests that the methodologies used here could be applied to a broad range of laser-modulated quantum materials, promising for applications including nonvolatile memory and ferroelectric field-effect transistors.

ACKNOWLEDGMENTS

This work was supported by the starting funding from National Center for Nanoscience and Technology. This work was supported by the National Key R&D Program of China (Grant No. 2022YFA1203200), the Basic Science Center Project of the National Natural Science Foundation of China (Grant No. 22388101), the Strategic Priority Research Program of the Chinese Academy of Sciences (Grant No. XDB36000000), and the National Natural Science Foundation of China (Grant No. 12125202). The numerical calculations in this study were partially carried out on the ORISE Supercomputer. We thank Q. Yang for fruitful discussions.

The authors declare no competing financial interest.

DATA AVAILABILITY

The data that support the findings of this article are not publicly available. The data are available from the authors upon reasonable request.

[1] A. I. Khan, A. Keshavarzi, and S. Datta, The future of ferroelectric field-effect transistor technology, Nat. Electron. **3**, 588 (2020).

[2] G. Feng, Q. Zhu, X. Liu, L. Chen, X. Zhao, J. Liu, S. Xiong, K. Shan, Z. Yang, Q. Bao, F. Yue, H. Peng, R. Huang, X. Tang, J. Jiang, W. Tang, X. Guo, J. Wang, A. Jiang, B. Dkhil *et al.*, A ferroelectric fin diode for robust non-volatile memory, Nat. Commun. **15**, 513 (2024).

[3] T. Li, A. Lipatov, H. Lu, H. Lee, J.-W. Lee, E. Torun, L. Wirtz, C.-B. Eom, J. Íñiguez, A. Sinitskii, and A. Gruverman, Optical control of polarization in ferroelectric heterostructures, Nat. Commun. **9**, 3344 (2018).

[4] J. F. Scott, Applications of modern ferroelectrics, Science **315**, 954 (2007).

[5] L. W. Martin and A. M. Rappe, Thin-film ferroelectric materials and their applications, Nat. Rev. Mater. **2**, 16087 (2016).

[6] D. Zhao, T. Lenz, G. H. Gelinck, P. Groen, D. Damjanovic, D. M. de Leeuw, and I. Katsouras, Depolarization of multidomain ferroelectric materials, Nat. Commun. **10**, 2547 (2019).

[7] M. D. Glinchuk, E. A. Eliseev, and V. A. Stephanovich, The depolarization field effect on the thin ferroelectric films properties, Phys. B (Amsterdam, Neth.) **322**, 356 (2002).

[8] X. Jin, Y.-Y. Zhang, and S. Du, Recent progress in the theoretical design of two-dimensional ferroelectric materials, Fundam. Res. **3**, 322 (2023).

[9] T. Li, Y. Wu, G. Yu, S. Li, Y. Ren, Y. Liu, J. Liu, H. Feng, Y. Deng, M. Chen, Z. Zhang, and T. Min, Realization of sextuple polarization states and interstate switching in antiferroelectric $CuInP_2S_6$, Nat. Commun. **15**, 2653 (2024).

[10] F. Liu, L. You, K. L. Seyler, X. Li, P. Yu, J. Lin, X. Wang, J. Zhou, H. Wang, H. He, S. T. Pantelides, W. Zhou, P. Sharma, X. Xu, P. M. Ajayan, J. Wang, and Z. Liu, Room-temperature ferroelectricity in $CuInP_2S_6$ ultrathin flakes, Nat. Commun. **7**, 12357 (2016).

[11] A. Belianinov, Q. He, A. Dziaugys, P. Maksymovych, E. Eliseev, A. Borisevich, A. Morozovska, J. Banys, Y. Vysochanskii, and S. V. Kalinin, $CuInP_2S_6$ room temperature layered ferroelectric, Nano Lett. **15**, 3808 (2015).

[12] J. A. Brehm, S. M. Neumayer, L. Tao, A. O'hara, M. Chyasnavichus, M. A. Susner, M. A. Mcguire, S. V. Kalinin, S. Jesse, P. Ganesh, S. T. Pantelides, P. Maksymovych, and N. Balke, Tunable quadruple-well ferroelectric van der Waals crystals, Nat. Mater. **19**, 43 (2020).

[13] A. Dziaugys, K. Kelley, J. A. Brehm, L. Tao, A. Puretzky, T. Feng, A. O'hara, S. Neumayer, M. Chyasnavichyus, E. A. Eliseev, J. Banys, Y. Vysochanskii, F. Ye, B. C. Chakoumakos, M. A. Susner, M. A. Mcguire, S. V. Kalinin, P. Ganesh, N. Balke, S. T. Pantelides *et al.*, Piezoelectric domain walls in van der Waals antiferroelectric $CuInP_2Se_6$, Nat. Commun. **11**, 3623 (2020).

[14] J. Wu, H.-Y. Chen, N. Yang, J. Cao, X. Yan, F. Liu, Q. Sun, X. Ling, J. Guo, and H. Wang, High tunnelling electroresistance in a ferroelectric van der Waals heterojunction via giant barrier height modulation, Nat. Electron. **3**, 466 (2020).

[15] L. You, Y. Zhang, S. Zhou, A. Chaturvedi, S. A. Morris, F. Liu, L. Chang, D. Ichinose, H. Funakubo, W. Hu, T. Wu, Z. Liu, S. Dong, and J. Wang, Origin of giant negative piezoelectricity in a layered van der Waals ferroelectric, Sci. Adv. **5**, eaav3780 (2019).

[16] Y. Li, J. Fu, X. Mao, C. Chen, H. Liu, M. Gong, and H. Zeng, Enhanced bulk photovoltaic effect in two-dimensional ferroelectric $CuInP_2S_6$, Nat. Commun. **12**, 5896 (2021).

[17] A. Simon, J. Ravez, V. Maisonneuve, C. Payen, and V. B. Cajipe, Paraelectric-ferroelectric transition in the lamellar thiophosphate $CuInP_2S_6$, Chem. Mater. **6**, 1575 (1994).

[18] D. Seleznev, S. Singh, J. Bonini, K. M. Rabe, and D. Vanderbilt, Cyclic ferroelectric switching and quantized charge transport in $CuInP_2S_6$, Phys. Rev. B **108**, L180101 (2023).

[19] Z. Zhou, S. Wang, Z. Zhou, Y. Hu, Q. Li, J. Xue, Z. Feng, Q. Yan, Z. Luo, Y. Weng, R. Tang, X. Su, F. Zheng, K. Okamoto, H. Funakubo, L. Kang, L. Fang, and L. You, Unconventional polarization fatigue in van der Waals layered ferroelectric ionic conductor $CuInP_2S_6$, Nat. Commun. **14**, 8254 (2023).

[20] W. Ding, J. Zhu, Z. Wang, Y. Gao, D. Xiao, Y. Gu, Z. Zhang, and W. Zhu, Prediction of intrinsic two-dimensional ferroelectrics in In_2Se_3 and other III2-VI3 van der Waals materials, Nat. Commun. **8**, 14956 (2017).

[21] V. Maisonneuve, V. B. Cajipe, A. Simon, R. Von Der Muhll, and J. Ravez, Ferrielectric ordering in lamellar $CuInP_2S_6$, Phys. Rev. B **56**, 10860 (1997).

[22] X. Yao, Y. Bai, C. Jin, X. Zhang, Q. Zheng, Z. Xu, L. Chen, S. Wang, Y. Liu, J. Wang, and J. Zhu, Anomalous polarization enhancement in a van der Waals ferroelectric material under pressure, Nat. Commun. **14**, 4301 (2023).

[23] X. Zhang, C. Xiao, Z. Zhang, L. Dong, H. Pan, C. Cao, S. A. Yang, S.-H. Wei, and Y. Lu, Origin of versatile polarization state in $CuInP_2S_6$, Phys. Rev. B **108**, L161406 (2023).

[24] S. N. Neal, S. Singh, X. Fang, C. Won, F.-T. Huang, S.-W. Cheong, K. M. Rabe, D. Vanderbilt, and J. L. Musfeldt, Vibrational properties of $CuInP_2S_6$ across the ferroelectric transition, Phys. Rev. B **105**, 075151 (2022).

[25] W. Ming, B. Huang, S. Zheng, Y. Bai, J. Wang, J. Wang, and J. Li, Flexoelectric engineering of van der Waals ferroelectric $CuInP_2S_6$, Sci. Adv. **8**, eabq1232 (2022).

[26] Y. Liu, Y. Wu, H. Han, Y. Wang, R. Peng, K. Liu, D. Yi, C.-W. Nan, and J. Ma, $CuInP_2S_6$-based electronic/optoelectronic synapse for artificial visual system application, Adv. Funct. Mater. **34**, 2306945 (2024).

[27] See Supplemental Material at http://link.aps.org/supplemental/10.1103/PhysRevB.111.104111 for methods and further analysis of the reported data, which includes Refs. [28–44].

[28] E. Runge and E. K. U. Gross, Density-functional theory for time-dependent systems, Phys. Rev. Lett. **52**, 997 (1984).

[29] S. Meng and E. Kaxiras, Real-time, local basis-set implementation of time-dependent density functional theory for excited state dynamics simulations, J. Chem. Phys. **129**, 054110 (2008).

[30] C. Lian, M. Guan, S. Hu, J. Zhang, and S. Meng, Photoexcitation in solids: first-principles quantum simulations by real-time TDDFT, Adv. Theory Simul. **1**, 1800055 (2018).

[31] P. Ordejón, E. Artacho, and J. M. Soler, Self-consistent order-N density-functional calculations for very large systems, Phys. Rev. B **53**, R10441 (1996).

[32] M. S. José, A. Emilio, D. G. Julian, G. Alberto, J. Javier, O. Pablo, and S.-P. Daniel, The SIESTA method for *ab initio* order-N materials simulation, J. Phys.: Condens. Matter **14**, 2745 (2002).

[33] D. Sánchez-Portal, P. Ordejón, E. Artacho, and J. M. Soler, Density-functional method for very large systems with LCAO basis sets, Int. J. Quantum Chem. **65**, 453 (1997).

[34] K. Yang, H. Wan, J. Yu, H. Fu, J. Zhang, X. Shi, and W. Fang, Interfacial polarization enhanced ultrafast carrier dynamics in ferroelectric $CuInP_2S_6$, Nano Lett. **25**, 1890 (2025).

[35] N. Troullier and J. L. Martins, Efficient pseudopotentials for plane-wave calculations, Phys. Rev. B **43**, 1993 (1991).

[36] C. Lian, Z. A. Ali, H. Kwon, and B. M. Wong, Indirect but efficient: laser-excited electrons can drive ultrafast polarization switching in ferroelectric materials, J. Phys. Chem. Lett. **10**, 3402 (2019).

[37] C. Song, Q. Yang, X. Liu, H. Zhao, C. Zhang, and S. Meng, Electronic origin of laser-induced ferroelectricity in $SrTiO_3$, J. Phys. Chem. Lett. **14**, 576 (2023).

[38] Q. Yang and S. Meng, Light-induced complete reversal of ferroelectric polarization in sliding ferroelectrics, Phys. Rev. Lett. **133**, 136902 (2024).

[39] R. D. King-Smith and D. Vanderbilt, Theory of polarization of crystalline solids, Phys. Rev. B **47**, 1651 (1993).

[40] G. Kresse and J. Hafner, *Ab initio* molecular dynamics for liquid metals, Phys. Rev. B **47**, 558 (1993).

[41] G. Kresse and J. Furthmüller, Efficient iterative schemes for ab initio total-energy calculations using a plane-wave basis set, Phys. Rev. B **54**, 11169 (1996).

[42] J. P. Perdew, J. A. Chevary, S. H. Vosko, K. A. Jackson, M. R. Pederson, D. J. Singh, and C. Fiolhais, Atoms, molecules, solids, and surfaces: Applications of the generalized gradient approximation for exchange and correlation, Phys. Rev. B **46**, 6671 (1992).

[43] P. E. Blöchl, Projector augmented-wave method, Phys. Rev. B **50**, 17953 (1994).

[44] B. Kaduk, T. Kowalczyk, and T. Van Voorhis, Constrained density functional theory, Chem. Rev. **112**, 321 (2012).